VII International Conference on Computational Methods for Coupled Problems in Science and Engineering
COUPLED PROBLEMS 2017
M. Papadrakakis, E. Oñate and B. Schrefler (Eds)

OPTIMIZATION OF A STRUCTURE UNDER INTENSE THERMAL RADIATION AND ITS SELF-WEIGHT

Nicolau José Moreno Velez*, Miguel António Lopes de Matos Neves† and Hugo Filipe Diniz Policarpo*†

*Instituto de Plasmas e Fusão Nuclear (IPFN)
Instituto Superior Técnico, Universidade de Lisboa
1049-001 Lisboa, Portugal
e-mails: hpolicarpo@ipfn.ist.utl.pt, nicolau.velez@ipfn.ist.utl.pt, web page:
http://www.ipfn.tecnico.ulisboa.pt

†LAETA, IDMEC
Instituto Superior Técnico, Universidade de Lisboa
1049-001 Lisboa, Portugal
e-mail: miguel.matos.neves@tecnico.ulisboa.pt - Web page:
https://www.idmec.ist.utl.pt/laeta/

Key words: Plasma Position Reflectometry (PPR), PPR Antenna, International Thermonuclear Experimental Reactor (ITER), Optimization, Radiation, Temperature Minimization, Displacement Minimization

Abstract. This proceeding presents work being developed to the optimization of thermoelastic structures under thermal radiation and its self-weight, involving thermal conductivity but not convection. For the analysis, it is used a thermal-structural finite element module of a commercial FE program where the radiation is modelled through view factors between elemental surfaces. The thermostructural problem under the assumption of small deformations is then treated as weak coupling problem. Limitations of the available tools are briefly discussed. For the optimization, a SIMP topology optimization (TO) is used to find optimized material distributions along a given spatial domain. The objective is to achieve both lower maximum temperature along the structure as well as lower maximum displacement. Some examples of results are presented for the long hollow truncated rectangle metallic pyramid analysed. The known effect that TO tends to remove most of the material in the design areas is firstly analysed. It is also presented a study of adding uniform coverage in thickness to reduce the maximum temperature and displacement, which resulted in an optimized solution with a small step near the end of the pyramid directly exposed to the radiation source. This somehow unexpected result is discussed.

1 INTRODUCTION

In the past few decades, the search for better structural performance has originated excellent results in the structural optimization field, namely optimization by material distribution. By optimizing the material distribution, a given structure will benefit from a relieve of unnecessary weight and an increase of its global stiffness.

The structure here studied is part of the PPR Diagnostics System [1] belonging to the ITER Tokamak. The PPR components presented are inside a vacuum chamber and therefore immersed in a quasi-vacuum environment. Furthermore, the components are exposed to a plasma radiative source that induces: i) direct heat loads, which will be radiate to the surrounding environment and transferred by conduction to other components in contact and, ii) indirect heat loads, arising from neutronics radiation, that are considered as internal heat generation in the structure.

The main concerns here are both the displacement and the high temperatures achieved as a result of the thermal expansion and the gravity acting on the bodies. Besides the attrition that the antenna will be subjected to, these issues can lead to oscillations/displacements of the structure that can originate clashes between components of the PPR, as well as material phase changes and consequently potential loss of the antennas functionality.

Optimizing a structure in order to minimize its temperatures can have multiple advantages. An example of temperature optimization by material distribution can be described by the components of Earth orbiting satellites, once these structures are also subjected to high amounts of energy coming from the nuclear fusion processes occurring in the Sun. By optimizing these satellites material distribution, besides decreasing maximum temperatures achieved, also the weight of the components may decrease, which would save a considerable amount of fuel spent during operations.

In the field of material distribution optimization, one of the most efficient existing methods is TO. This method, which finds optimized material distribution through element density redistribution, has been studied intensively and many work use the method Solid Isotropic Material with Penalization (SIMP). The initial work is due to Bendsøe and Kikuchi [2] and substantial information can be seen in Sigmund [3] and, in a more embracing way in [4] by Sigmund and Bendsøe. These authors were responsible for introducing this kind of structural optimization, giving way for the creation of new and improved methods. Still, there are not many works in thermoelastic structures with TO as far as their authors knowledge, but just to refer some works as Rodrigues and Fernandes [5], Bruns [6], Deaton [7] and Ricardo et al [8].

This proceeding presents methods being studied to perform material distribution optimization of the ITER PPR Antenna, aiming to decrease both its maximum temperature achieved during the thermal process and the resulting displacements. For that purpose, two main paths are followed. One consists in parametric studies using Finite Element Analysis (FEA) and Adaptive Single Objective (ASO) or Adaptive Multiple Objective

(AMO), implemented in the commercial code used here [9]. The other path consists in using a modified SIMP optimization method, which, besides the displacement optimization, also allows for optimization with temperature objectives.

The techniques applied in the parametric optimization resulted in curious and may be promising outcomes, where both minimized temperature and displacement were achieved.

2 METHODOLOGY

2.1 Thermoelastic problem

The thermoelastic structural analysis is performed as a weakly coupled problem, where first a thermal analysis is conducted with the resulting temperatures being imported to a static analysis (in a unidirectional path). This two-step procedure is suited as temperature influences displacement but the opposite is considered negligible.

Regarding the thermal process, the Hooke's law is applied as:

$$\{\sigma^t\} = [E]\{\varepsilon^t\}, \tag{1}$$

where $\{\sigma^t\}$ is the thermal stresses vector, $[E]$ is the elasticity matrix and $\{\varepsilon^t\}$ is the thermal strain vector.

2.2 Heat transfer problem

The conduction process is solved according to the Fourier's Law:

$$q = -\frac{\Delta T}{R_{cond}}, \tag{2}$$

where ΔT is the temperature difference between two surfaces and R_{cond} the thermal resistance in conduction.

Regarding the radiation process, the amount of energy that reaches a given surface (area) j will be conditioned by the way this surface is disposed towards the emitter one i. This value can be measured by the view factor F_{ij} and its calculation by computational methods can be done through the Nusselt's hemicube method [10] as seen in the hemicube schematic in Fig.1 (where ϕ represents the angle and the hemicube sides are subdivided into N grid cells, named pixels). Following this, the view factor are achieved as:

$$F_{ji} = \sum_{j=1}^{N} \frac{cos(\phi_i)cos(\phi_j)}{\pi R_{ij}^2} \Delta A_j, \tag{3}$$

with N being the number of pixels created, ΔF_n the view factor between the reference surface and each of the target pixels, ϕ_i and ϕ_j the angles between the surfaces and R_{ij} the direct length between the centroid points of the two surfaces.

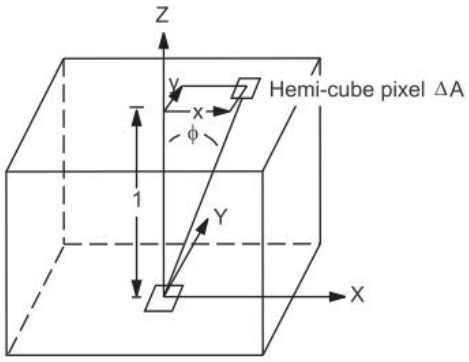

Figure 1: Schematic representation of the hemicube method present in [10].

2.3 Finite element analysis via weak coupling

Regarding the heat transfer, the FEA solves the following equation:

$$\begin{aligned} &[\mathrm{C}]\{\dot{\mathrm{T}}\} + [\mathrm{K}_T]\{\mathrm{T}\} = \{\mathrm{R}_T\} \\ &[\mathrm{K}_T] = [\mathrm{K}_k] + [\mathrm{H}_{conv}] + [\mathrm{H}_{rad}] \\ &\{\mathrm{R}_T\} = \{\mathrm{R}_B\} + \{\mathrm{R}_{hconv}\} + \{\mathrm{R}_{h_{rad}}\} + \{\mathrm{R}_Q\} \end{aligned} \tag{4}$$

where [C] and $[\mathrm{K}_T]$ are the general global specific heat and conductivity matrices, and $\{\mathrm{R}_T\}$, $\{\mathrm{T}\}$ and $\{\dot{\mathrm{T}}\}$ are the general global thermal load, temperature, and the first derivative of the temperature vectors, respectively. Furthermore, $[\mathrm{K}_k]$, $[\mathrm{H}_{conv}]$ and $[\mathrm{H}_{rad}]$ are the global conductivity, convection and radiation matrices, and $\{\mathrm{R}_B\}$, $\{\mathrm{R}_h\}$ and $\{\mathrm{R}_{h_{rad}}\}$ are the global heat flux, convection, radiation and heat generation vectors, respectively. The FEA is established as a nonlinear transient thermal analysis (as radiation is considered and the properties of the materials are temperature dependent) that considers conduction and radiation effects (convection is not considered as the medium is vacuum, which means that $[\mathrm{H}_{conv}] = \{\mathrm{R}_{hconv}\} = 0$) to estimate the temperature distribution along the antenna.

A Steady-State Thermal analysis is performed and followed by a structural elastostatic/steady state analysis:

$$[\mathrm{K}]\{U\} = \{F\} + \{F^{th}\} \tag{5}$$

where, [K] is the global stiffness matrix, $\{F\}$ is the global mechanical load vector, $\{F^{th}\}$ is the global thermal load vector and $\{U\}$ is the global displacement vector.

2.4 Thermostructural analysis

A CAD model of the antenna, is illustrated in Fig. 2 with the respective dimensions: w-width, h-height, t-thickness (uniform) and L-length, presented in Table 1.

In Fig.3 a), the complete model used in both thermal and static analyses is illustrated, where the antenna is located between two blankets and directly faced towards a plasma surface. In this model, a constant temperature of 300 °C [11] is applied to the rear side of

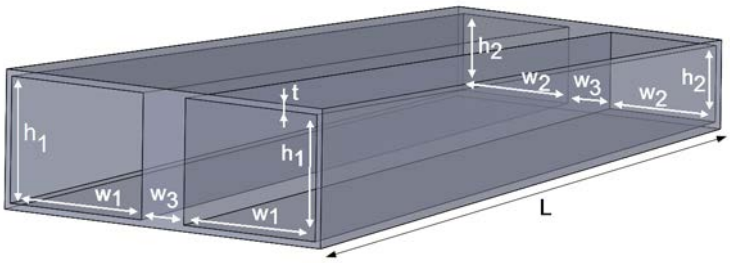

Figure 2: CAD model of ITER PPR antenna (index 1-front, 2-rear).

Table 1: Dimensions (in mm) of the ITER PPR antenna.

w_1	w_2	w_3	h_1	h_2	t	L
25	20	8	20	12	1	115.4

the antenna, where it is structurally fixed, and to the inner surface of the blanket surfaces. An earth gravity acceleration of 9,8066 m/s^2 is considered, acting on a direction parallel ($-z$ axis in Fig.3 b)) to the rear face of the antenna.

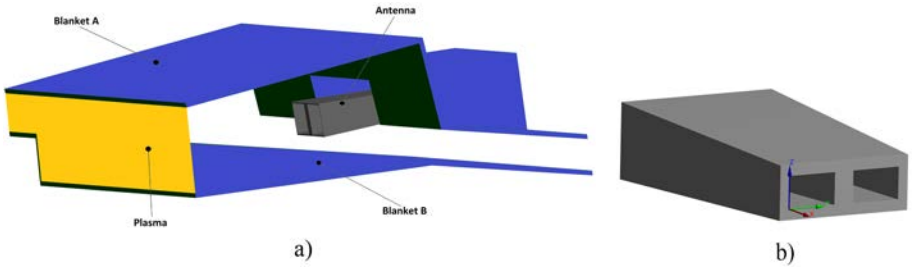

Figure 3: Radiation enclosure model in a) and antenna coordinate system in b).

An initial Steady State Thermal analysis was performed on the model, using the Ansys Workbench software, considering this as the worst case scenario, i.e., when the maximum temperatures will be higher.

From the original antenna FE model, a new model is created (as seen in Fig.4) to perform design optimization and parametric studies.

In the model presented in Fig.4 the illustrated parameters L_c and t_c are respectively the length and thickness of the antenna coverage. This FE model features 3D 20-node structural-thermal FEs with a four degree-of-freedom at each node and 3D radiosity surface FEs for radiosity, overlaid on the exposed face of the 3D thermal FEs.

2.5 Optimization

The structure was subjected to two kinds of optimization: Topology Optimization and Parametric Optimization.

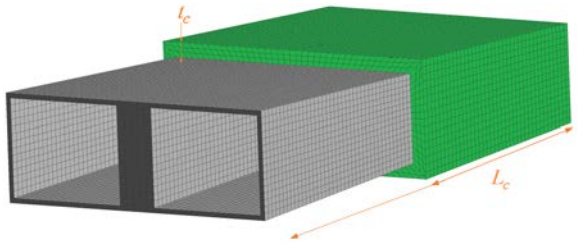

Figure 4: Parameterized CAD model: (w width; h - height, t - thickness (uniform) and L - length).

In the first case, a modified approach of the SIMP is applied to the antenna using:

$$E_i = E_{min} + \rho_i^p (E_0 - E_{min}),\ \rho \in]0, 1] \tag{6}$$

with E_0 being the elastic properties of the solid material, ρ the element relative density, E_i the element elastic properties and E_{min} the elastic property of the "void" material. This allows for the maximization of the material stiffness, which is obtained by searching the best material distribution through compliance or elastic strain energy $\mathbf{C}$ minimization:

$$\begin{aligned} & find\{\boldsymbol{\rho}\} = (\rho_1, .., \rho_i, .., \rho_{n_d}), 0 < \rho_i \leq 1, i = 1, .., n_d \\ & min[\mathbf{C}] = \frac{1}{2}(\{\mathbf{f}\} + \{\mathbf{G}\})^T \{\mathbf{u}\} \\ & s.t. \\ & \{\mathbf{f}\} + \{\mathbf{G}\} = [\mathbf{K}]\{\mathbf{u}\} \\ & V \leq V_{(U)} \end{aligned} \tag{7}$$

where ρ_i is the pseudo-density variables, n_d is the number of densities variables, $\mathbf{f}$ is the thermal load vector, $\mathbf{G}$ the self-weight load vector, $\mathbf{u}$ is the nodal displacement vector and $\mathbf{K}$ is the structural global stiffness matrix. Furthermore, V is the total volume of the material used for the structure and $V_{(U)}$ is the prescribed upper limit.

In the second case, a parametric optimization is performed using available algorithms in the commercial code used. The process is managed by the necessity of having one or more objectives, which will translate in ASO or AMO algorithms, respectively [12].

Since the primal objective of this study is to decrease the maximum temperatures achieved in the antenna while subjected to the operating conditions, the first step is to perform a single objective optimization, i.e., ASO.

On the other hand, even if having minor impact on the project, also the structure displacement is of great importance, which leads to the multiobjective optimization AMO. Here both temperature and displacements are minimized, demanding weights to be attributed to both objectives

3 RESULTS AND DISCUSSION

3.1 A brief verification

To check the procedure used with the TO technique, the curiously named Shape Optimization BETA tool from ANSYS Workbench is used. So, before using the TO commercial tool in the antenna problem, first a verification test was made relatively to the results in [13], where a simple temperature variation is imposed on a clamped-clamped 2D structure subjected to a vertical centered force and a volume constraint of 40%, as illustrated in Fig.5.

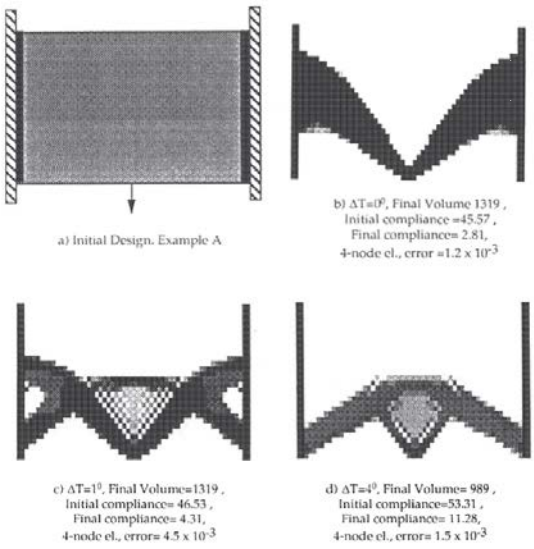

Figure 5: Topology Optimization in thermally loaded structure in [13] for $\Delta T=0°$, $\Delta T=1°$ and $\Delta T=4°$.

Using the already mentioned TO ANSYS tool, the obtained results with the exact same constraints as in [13] are the following (Fig.6).

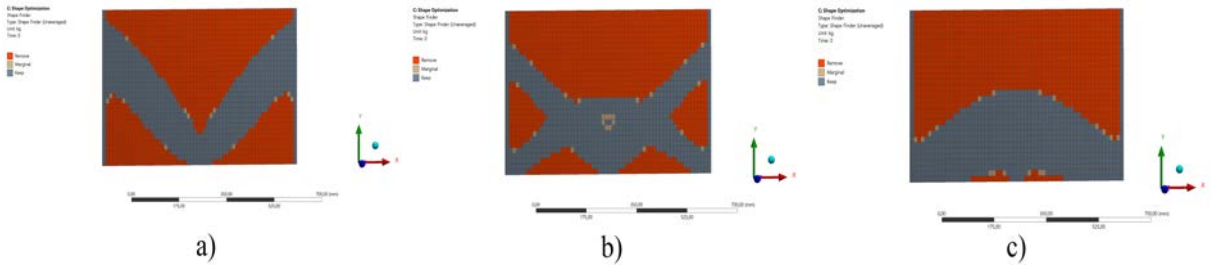

Figure 6: TO results obtained with TO ANSYS tool for a)-$\Delta T=0°$, b)-$\Delta T=1°$ and c)-$\Delta T=4°$.

By observing Fig.6, it is possible to state that all three outcomes based on each ΔT are similar to the ones presented in the mentioned work.

3.2 Application of optimization to the antenna

With this being said, the results obtained when applying this method to the antenna model result in two different solutions, both with a volume constraint of 50%, as follows in Fig.7.

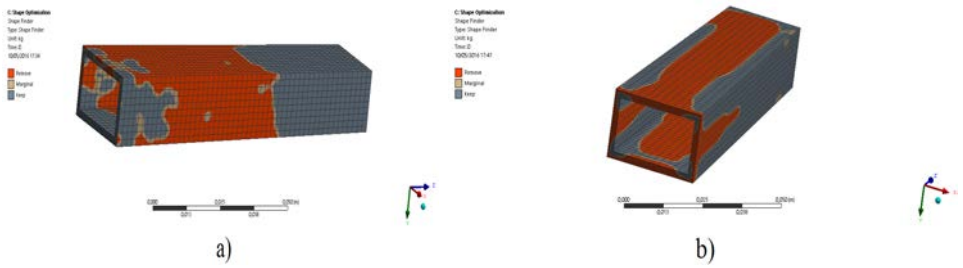

Figure 7: Examples of TO application to the antenna.

Looking at Fig.7, one can see that both results obtained are unwanted. This happens once material from the internal faces is removed, which eliminates the antenna's purpose, given the fact that these internal faces are crucial for the signal propagation.

Therefore, at this step, this TO software reveals itself as inappropriate for the work here being developed.

Regarding the thermostructural analysis, both the results are illustrated in Fig. 8. In Fig. 8 a), the maximum temperatures (T_{max}) along the antenna are portrayed, where one can see that they reach its peak in the frontal face of the antenna, as expected.

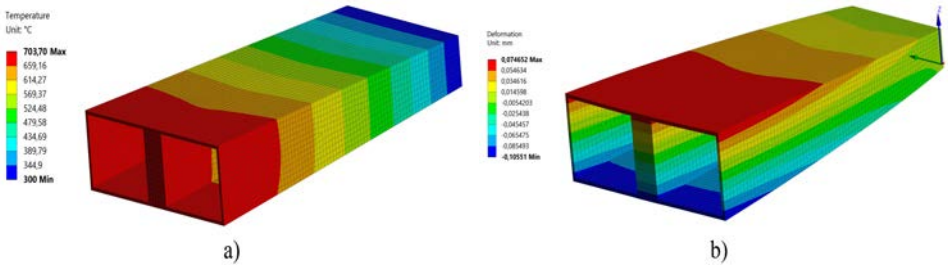

Figure 8: Results for thermostructural analyses: a) Temperature distribution and b) Displacement distribution

Respecting Fig. 8 b), the results for maximum displacement (D_{max}) along the antenna are displayed, where it can be seen that the maximum value also occurs in the frontal part of the antenna, which, given the problem constraints (Fig.3), is what should be expected. This is the first region, of the PPR in-vessel system, facing the plasma, hence the first to be in contact with the plasma loads, reaching a of $\sim 704°C$, a mean temperature of $\sim 557°C$ and a (thermal expansion and displacements due to its dead weight) of $\sim 0,106mm$.

Following this, in Fig.9 are presented the results for the parametric studies, with respect to T_{max} and D_{max}, showing the evolution of these values with the increase of the antenna coverage.

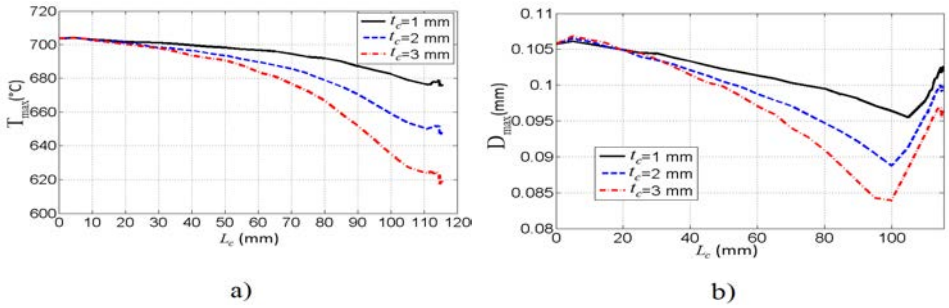

Figure 9: Results for parametric studies: a) temperature and b) displacement.

Looking at both results in Fig.9, it is possible to infer that T_{max} and D_{max} decrease with the coverage increase, until a given point near the full coverage condition. In Fig.9 a), T_{max} decreases until a minimum point located somewhere between $114 \leq L_c \leq 115.4$mm and for maximum thickness (t_c=3mm). In fig.9 b), D_{max} is located somewhere between $95 \leq L_c \leq 110$, also for a maximum value of thickness. With the results of these studies, the optimization action zones are established. Given the importance of T_{max}, a interval of $114 \leq L_c \leq 115.4$mm and maximum thickness for the ASO feature and a combined interval of $95 \leq L_c \leq 115.4$mm and $t_c = 3$mm for the AMO giving T_{max} and D_{max} the same objective weight. The results for the ASO are illustrated in Fig.10, where the minimum T_{max} of 617.3 °C is obtained for $L_c = 114.7$mm, corresponding to 0.7mm from the front edge, originating the CAD model in Fig.11 a).

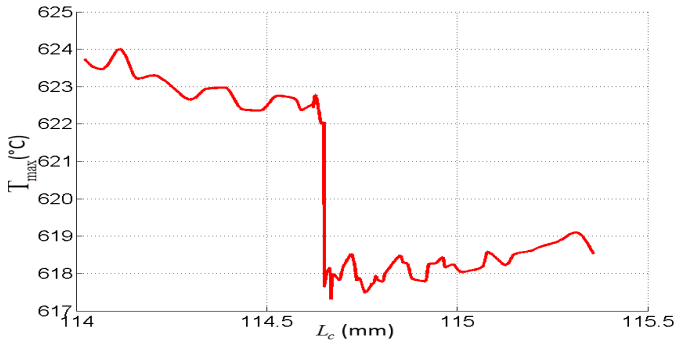

Figure 10: Plot of parametric study of T_{max} in function of L_c

In Fig.12 the results for the AMO are presented, where a Pareto front illustrates the values obtained for an equal weight of 50% for T_{max} and D_{max} as a function of L_c and $t_c = 3$mm. The best value obtained is for $L_c = 102.8$mm, as it is the point where both

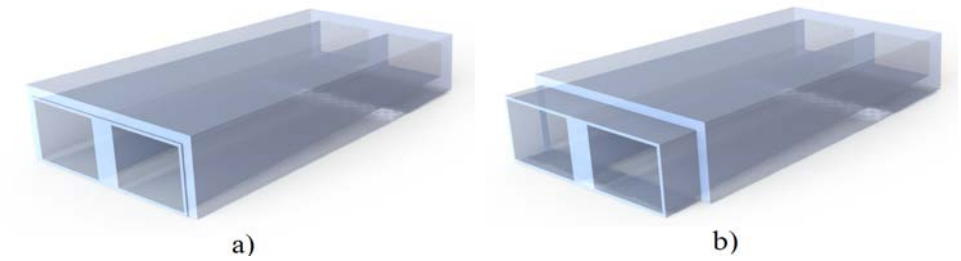

Figure 11: Resulting CAD models from ASO (a)) and AMO (b)) features.

temperature and displacement reveal the best balance of low values. This value presents results of $T_{max} = 631.9°C$ and $D_{max} = 0.087mm$, corresponding to a distance of 12.6 mm from the front edge of the antenna, originating the CAD model illustrated in Fig.11 b).

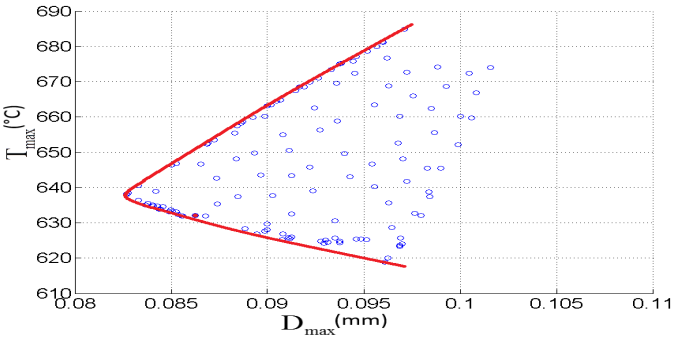

Figure 12: Plot of results from AMO feature.

Both parametric optimization cases reveal improvements in their objectives, which are summarized in Table 2, where results are compared to initial values and is the average temperature of the antenna.

Table 2: Initial and optimized results obtained by ASO and AMO.

	L_c (mm)	t_c (mm)	T_{max} °C	T_{mean} °C	D_{max} (mm)
Initial	0	0	703.7	556.7	0.106
ASO	114.7	3	617.3	500.5	-
AMO	102.8	3	631.9	492.6	0.087

From the data included in Table 2, one can see a decrease in T_{max} and T_{mean} of 86.4°C (12.3%) and 56.2°C (10.1%), respectively in the ASO case. Regarding the AMO case, a decrease in , and of 71.8°C (10.2%), 64.1°C (11.5%) and 0.019 mm (17.9%), respectively is evidenced.

The decreases in temperature are explained by the increase of the heat flux by conduction given the increase in material along the antenna. This phenomenon allied with the structure exposure to the plasma heat radiation leads to the best result at 0,7mm from a full coverage.

In respect to the decrease in D_{max}, it is associated to the gain of structural stiffness by adding material to the rear part of the antenna, restraining its movements.

4 CONCLUSIONS

- This study is at a preliminary step and results need to be better interpreted.
- In this work, several optimization methods, namely TO, ASO and AMO, were used.
- The results obtained for the PPR antenna with the ANSYS TO tool, revealed inappropriate results as one concludes that it does not account for thermal radiation exchanges. This motivated the use of parametric studies ASO and AMO.
- The parametric studies of the antenna indicate that and decrease with the increase of and until the optimum. With ASO one obtains and decrease of 12.3% and 10.1%, respectively and with AMO one obtains a, and of 10.2%, 11.5% and 17.9%.
- With lower values of and, the lifetime of the antenna is extended, less maintainability is required and hence, the availability of the antenna is increased. With lower, the signal attenuation is improved and more accurate estimations for the plasma position are expected.
- Note that this is a preliminary study that needs further improvements regarding the ASO optimum solution. Regarding TO, there are some promising studies in the area that deal with conduction and radiation problems. However, they are still embryonic and not available in commercial codes as far as the knowledge of the authors.

REFERENCES

[1] Varela, P. *55.F3 PPR: System Design Description Document (DDD), ITER_D_SGCQ2S v2.0, July 2016.*

[2] Bendsøe, M.P. and Kikuchi, N. *Generating Optimal Topologies in Structural Design Using a Homogenization Method.* Computer Methods in Applied Mechanics and Engineering 71 (1988).

[3] Sigmund, O. *Design of material structures using topology optimization.* CPh.D. Thesis, Department of Solid Mechanics, Technical University of Denmark, (1994).

[4] Bendsøe, M.P. and Sigmund, O. *Topology Optimization - Theory, Methods, and Applications.* Springer, 2^{nd} edition (2003).

[5] Rodrigues, H. and Fernandes, P. *A material based model for topology optimization of thermoelastic structures*. International Journal for Numerical Methods in Engineering , vol. 38, no. 12, pp. 19511965 (199).

[6] Bruns, T.E. *Topology optimization of convection-dominated, steady-state heat transfer problems*. International Journal of Heat and Mass Transfer, Vol. 50, pp. 2859-2873 (2007).

[7] Deaton, J.D. *Design of Thermal Structures using Topology Optimization*. PhD Thesis, Wright State University, (2009). (Online at http://cecs.wright.edu/cepro/docs/thesis/ Design_of_Thermal_Structures_using_Topology_Optimization_DEATON_2014.pdf).

[8] Ricardo, J. D. R., Coe, G., Carvalho, J. P., Branco, M. B. C., Barroqueiro, B., Abraos, P. and Neves, M. M. *Innovative cork application on a thermal deflector for apogee boost motors*. in the proceedings of the 14th European Conference on Spacecraft Structures, Materials and Environmental Testing (ECSSMET), 27-30 September, Toulouse, France (2016).

[9] *ANSYS Academic Research Help Manual*. Release 17.0 (2016).

[10] *Theory Reference for the Mechanical APDL and Mechanical Applications*. ANSYS, version 12.1, (2009).

[11] Policarpo, H. *F4E-FPA-375-SG04: Plan for the Thermal Analysis of the PPR Invessel Components*. F4E_D_25B8L7 v1.1 (2016).

[12] *Ansys DesignXplorer User's Guide v17,*. (2016).

[13] Rodrigues, H. and Fernandes, P. *Topology optimal design of thermoelastic structures using a homogenization method*. Control and Cybernetics, Vol.23, (1994).